



Geophysical Research Letters*



RESEARCH LETTER

10.1029/2023GL107822

Key Points:

- Electron zebra stripes are a persistent feature in Earth's inner magnetosphere, although they become intensified during geomagnetic storms
- Peak-valley ratio (∆j) in detrended electron flux within the zebra stripes enhances by ≥1 factor at L = 1.5 during three geomagnetic storms
- \(\Delta \) is well correlated with the net field-aligned current (FAC) in polar region, suggesting the dominant role of convection driven by FAC

Correspondence to:

M. Pandya, megha.phy14@gmail.com

Citation:

Pandya, M., Ebihara, Y., Tanaka, T., Manweiler, J. W., & Vines, S. K. (2024). Intensification of the electron zebra stripes in the Earth's inner magnetosphere during geomagnetic storms. *Geophysical Research Letters*, *51*, e2023GL107822. https://doi.org/10.1029/2023GL107822

Received 11 DEC 2023 Accepted 22 DEC 2023

© 2024 The Authors.

This is an open access article under the terms of the Creative Commons Attribution-NonCommercial License, which permits use, distribution and reproduction in any medium, provided the original work is properly cited and is not used for commercial purposes.

Intensification of the Electron Zebra Stripes in the Earth's Inner Magnetosphere During Geomagnetic Storms

Megha Pandya^{1,2,3}, Yusuke Ebihara¹, Takashi Tanaka⁴, Jerry W. Manweiler⁵, and Sarah K. Vines⁶

¹Research Institute for Sustainable Humanosphere, Kyoto University, Uji, Japan, ²Department of Physics, The Catholic University of America, Washington, DC, USA, ³NASA Goddard Space Flight Center, Greenbelt, MD, USA, ⁴International Research Center for Space and Planetary Environmental Science, Kyushu University, Fukuoka, Japan, ⁵Fundamental Technologies, LLC, Lawrence, KS, USA, ⁶John Hopkins University Applied Physics Laboratory, Laurel, MD, USA

Abstract We examined rapid variations in the electron zebra stripe patterns, specifically at L = 1.5, over a three-month duration, using twin Van Allen Probes within Earth's inner magnetosphere. During geomagnetically quiet intervals, these stripes exhibit a peak-to-valley ratio $(\Delta j) \sim 1.25$ in detrended electron fluxes. However, during geomagnetic storms, they became highly prominent, with $\Delta j > 2.5$. The correlation between Δj and net field-aligned currents (FACs) is observed to be high (0.70). Global magnetohydrodynamic (MHD) simulation results indicate that the westward electric field at midnight at low latitudes in the deep inner magnetosphere correlates well with net FACs. An increase in net FACs could amplify the dawn-to-dusk electric field in the deep inner magnetosphere, thereby causing the inward transport of electrons. Given that FACs are linked to the interaction between solar wind and the magnetosphere, our findings emphasize the importance of solar wind-magnetosphere coupling in the deeper regions of the inner magnetosphere.

Plain Language Summary The intensity of hundreds of keV electron fluxes displays a distinctive pattern in the energy versus L-value spectrogram, characterized by periodic valleys and peaks, commonly referred to as zebra stripes. These patterns have been observed in the magnetospheres of multiple planets, including Earth, Jupiter, and Saturn. Our study reveals that during geomagnetically quiet intervals, Earth's inner magnetospheric zebra stripes exhibit well-defined banded features. However, these bands become highly pronounced during geomagnetic storms. The peak-to-valley ratio (Δj) of detrended electron fluxes shows a correlation with net field-aligned currents (FACs), and these FACs, in turn, align with the westward component of the electric field at midnight. Consequently, FACs play a significant role in controlling electron flux dynamics deep within the inner magnetosphere. This research illuminates the solar wind-magnetosphere-ionosphere couplings.

1. Introduction

The energy versus L-value spectrogram for electron fluxes in the range of tens to hundreds of keV displays a regular, dominant pattern of band-like structures when L < 2.5 (Datlowe et al., 1985; Imhof et al., 1981a, 1981b; Sauvaud et al., 2013). These distinctive patterns were recently recorded in Earth's inner radiation belt by the Van Allen Probes satellite and have been termed "zebra stripes" (Ukhorskiy et al., 2014). Similar patterns of zebra stripes have been observed in the electron radiation belts of Saturn and Jupiter (Hao et al., 2020; Sun et al., 2021, 2022).

Over the years, multiple theories have been proposed to explain the formation and evolution of these electron zebra stripes in Earth's magnetosphere (Cladis, 1966; Lejosne & Roederer, 2016; Liu et al., 2016; Sauvaud et al., 2013; Ukhorskiy et al., 2014). Verifying these theories has been challenging due to the limited availability of in situ electric field measurements within Earth's inner radiation belt. Near perigee, both the strength of Earth's magnetic field and the velocity of the spacecraft are high, leading to a significant motional electric field. Although isolating this motional electric field has revealed intriguing geophysical electric fields in an inertial reference frame, complete removal becomes increasingly difficult when L < 3 (Breneman et al., 2022). This challenge in acquiring reliable electric field measurements close to the magnetic equator of the inner radiation belt is well-documented (Lejosne & Mozer, 2016a, 2016b). As a result, it remains difficult to rigorously test models based on electric field data, leaving the generation mechanism of zebra stripes largely unresolved.

This study builds upon earlier research on electron zebra stripes conducted by Pandya et al. (2023). Their work focused on modeling the evolution of electron zebra stripes through advection, using time-dependent electric fields generated from global magnetohydrodynamic (MHD) simulations. They discovered that the peaks in zebra stripes resulted from intensified westward electric field transients occurring in the pre-midnight to post-dawn region. However, they did not identify the source of these westward electric fields, which are crucial for the formation of zebra stripes. In our current study, we carry out a comprehensive long-term analysis of electron zebra stripes, utilizing data from the Radiation Belt Storm Probes Ion Composition Experiment (RBSPICE) instrument onboard the Van Allen Probes. We focus on both geomagnetically quiet and disturbed periods, examining variations in the intensity of electron fluxes in relation to changes in field-aligned currents (FACs). Section 2 outlines the satellite data and the methodology employed for identifying distinct zebra-stripe patterns, along with the physical parameters utilized in our simulations. Section 3 discusses our observations and analyses of the zebra stripes, while Section 4 delves into the underlying mechanisms responsible for their formation and the root causes of the associated electric fields. These findings are summarized in Section 5.

2. Data and Methodology

2.1. Satellite Data

We employed pitch-angle-resolved electron differential flux data captured by the RBSPICE instrument (Manweiler et al., 2022; Mitchell et al., 2013) on board the Van Allen Probe spacecraft. This spacecraft orbits Earth with a period of \sim 9 hr at an inclination of \sim 10° (Mauk et al., 2012), scanning plasma populations from a perigee of \sim 700 km to an apogee of \sim 6 Earth radii (R_E). The high-energy, low-time-resolution electron species rate (ESRHELT) product records electron fluxes ranging from approximately 25 keV to \sim 1 MeV across 64 logarithmically spaced energy bins and 17 pitch angles.

The Active Magnetosphere and Planetary Electrodynamic Response Experiment (AMPERE) observes FACs using data from the Iridium satellite constellation. Comprising over 70 commercial satellites, the Iridium network orbits Earth at an altitude of 780 km (Anderson et al., 2000). These satellites are evenly spaced about 2 hr apart in Magnetic Local Time (MLT) and are distributed across six orbital planes. Each Iridium satellite is equipped with a magnetometer, transmitting data to Earth at a lower resolution. A minimum of 1 hour of data accumulation is necessary for a rough estimation of FACs, which precludes measurements of reconnection events but allows for the assessment of large-scale Birkeland currents.

The Iridium data (Anderson et al., 2000) enables the identification of the average configuration of large-scale Birkeland currents. However, AMPERE's high-resolution data allows for the study of smaller, more intricate features within these currents. Previous studies from Anderson et al. (2000, 2002) have shown that by using 2-hr of magnetic field data from all satellites, it is possible to calculate global radial current densities via Ampere's law. At magnetic latitudes above 60°, these radial currents are termed FACs and are generally linked to the Region 1 (R1) and Region 2 (R2) current systems (Cowley, 2000; Iijima & Potemra, 1978). The data, collected in 10-min intervals and assessed every 2 min, were organized on a grid with a latitude resolution of 1° and an MLT resolution of 1 hr. Given the greater accuracy of Iridium's current distribution measurements in the Northern Hemisphere (Anderson et al., 2008), our analysis specifically focused on data from that region.

2.2. Detection of Zebra Stripe Pattern

We selected data from March 2015, June 2015, and September 2017, corresponding to three major geomagnetic storms of solar cycle 24. A spectrogram was used to delineate the relationship between energy and L-value, facilitating the identification of electron zebra stripes. We obtained detrended electron fluxes to discern the distinct peaks and valleys in these stripes, using the methodology outlined previously (Liu et al., 2016). The illustration of the technique for detrending the electron fluxes recorded on 8 September 2017, is detailed in Figure 1. Figure 1a presents a map contrasting energy with L-value for electron fluxes recorded at a 90° pitch angle by the RBSPICE instrument onboard Van Allen Probe-A. Figure 1b depicts the electron flux after smoothing over energy and L-value dimensions. In this context, the smoothed electron flux is calculated by taking the running average of the electron fluxes over a range of ± 4 energy bins, centered on a specific energy channel at a particular moment in time. Figure 1c shows detrended electron fluxes obtained by subtracting the smoothed fluxes from the observed ones for given energy and L-values. For a comprehensive long-term analysis, we examined detrended electron

PANDYA ET AL. 2 of 9

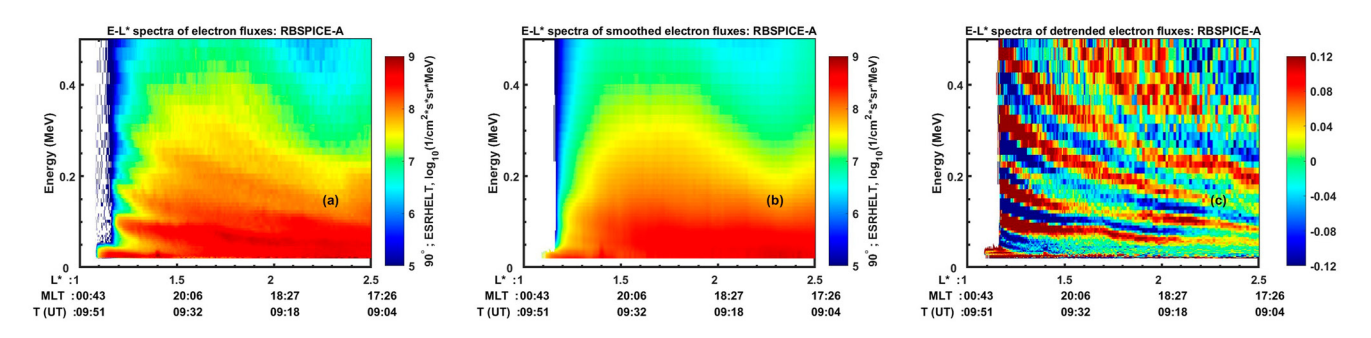


Figure 1. Illustration of the technique for detrending electron fluxes during the inbound passage of Van Allen Probe-A from 05:21 to 09:51 UT on 8 September 2017. Panel (a) displays the energy versus L-value spectrogram of logarithmically scaled electron fluxes at a 90° pitch angle. Panel (b) presents the energy versus L-value spectrogram for smoothed electron fluxes. Panel (c) illustrates the energy versus L-value spectrogram for the detrended electron fluxes.

fluxes in the zebra stripes over an entire month. We isolated each inbound and outbound satellite passage and applied the detrending algorithm to each. Our analysis primarily focused on a narrow range of L-values centered at 1.5. To quantify the variability of the peak-to-valley electron fluxes at $L \sim 1.5$, we calculate the parameter Δj , which presents the ratio of averaged detrended peak fluxes (j_p) to averaged detrended valley fluxes (j_p) in the energy range of 0.1–0.45 MeV at a given time.

2.3. Global MHD Simulation

The global magnetohydrodynamic (MHD) simulation employed in this study was developed by Tanaka (2015). It utilizes a total variation diminishing (TVD) scheme, which is particularly effective in capturing the interaction between supersonic plasma flow and dipole fields. The simulation employs a grid structure based on a three-dimensional sphere with 12 equal pentagonal faces, as described in previous studies (Moriguchi et al., 2008; Terada et al., 2009). At Level-1, each pentagonal face of the sphere is subdivided into five triangles, yielding 60 triangles across the entire sphere. At Level-2, each of these triangles is further divided into four smaller triangles, resulting in a total of 240 triangles. This subdivision process continues up to Level-6, ultimately generating 61,440 triangles. A 3D grid is then constructed by aligning 360 spheres between the inner boundary at 2.6 R_E and the outer boundary at 200 R_F at midnight, with the outer boundary extending to 600 R_F at noon. Assume that the magnetic field is dipole inside the inner boundary, we mapped the FACs from the inner boundary of the grid system to the ionosphere. To compute ionospheric conductivity, we considered contributions from solar extreme ultraviolet (EUV) radiation as well as from discrete and diffuse auroras. Given the FACs and the ionospheric conductivity, we solved the elliptic differential equation to ensure the continuity of ionospheric currents, and derived the electric potential. Despite the FAC being obtained at L-values greater than 2.6, we can derive the electric potential from pole to pole. Assuming that the Earth's magnetic field lines are equipotential, we mapped the resulting electric field onto the inner boundary of the magnetosphere to establish the inner boundary condition for the plasma flow. A comprehensive calculation of ionospheric conductivity and an example of the electric potential from pole to pole are provided by Ebihara et al. (2014).

3. Observation and Analysis

Figure 2a1 displays the energy-time spectrogram of detrended electron fluxes for a 90° pitch angle throughout March 2015. Each vertical slice signifies the electron flux recorded at $L = 1.5 \pm 0.02$. For enhanced spatial resolution, we integrated electron flux data from both the RBSPICE instrument onboard Van Allen Probe-A and Van Allen Probe-B into a single panel. Optimal stripe width of ± 15 min was selected to prevent overlap between adjacent stripes. Each vertical slice featured multiple peaks, appearing as zebra-like stripes. Notably, a very small color contrast features have emerged in the peak-to-valley values of detrended electron fluxes between 4 March and 16 March 2015. These band-like structures occasionally exhibited abrupt variations in time and energy. For example, a sudden increase in peak-to-valley values of detrended electron flux occurred from 17 March to early on 19 March 2015. Similar enhancements were also observed from 1 to 3 March 2015, coinciding with a minor solar storm. Electron flux intensities remained generally low to medium for the rest of the period. Figure 2b1 depicts the total magnitude of upward FACs in the Northern Hemisphere. A significant surge in FACs, reaching

PANDYA ET AL. 3 of 9

19448007, 2024, 3, Downloaded from https://agupubs.onlinelibrary.wiley.com/doi/10.1029/2023GL107822 by Southwest Research Institute, Wiley Online Library on [02/05/2024]. See the Terms and Conditions (https://online

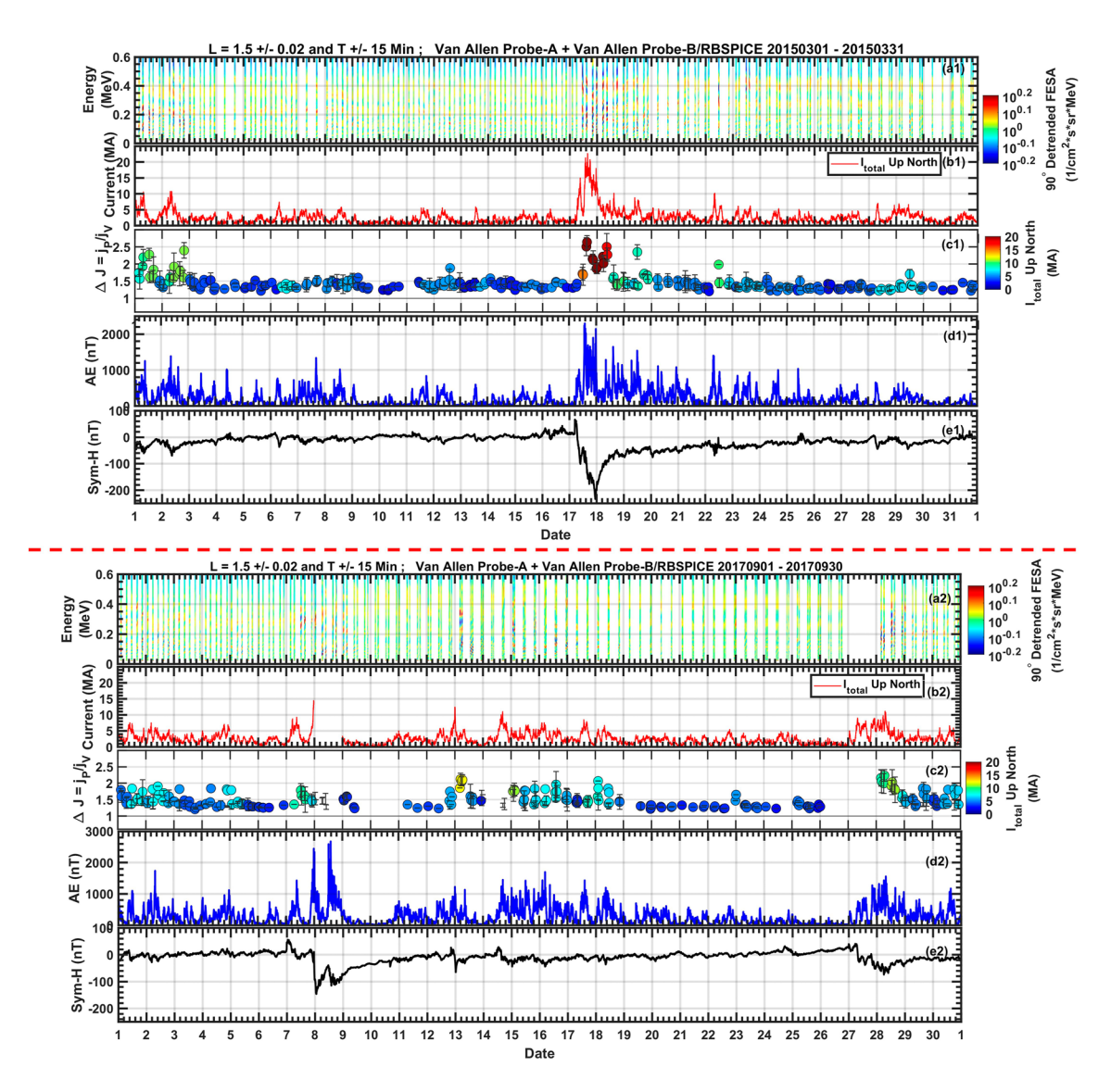


Figure 2. Energy-versus-time spectra of detrended electron fluxes at a 90° pitch angle for the entire months of (a1) March 2015 and (a2) September 2017, as recorded by RBSP-A and RBSP-B. Each stripe represents the intensity of electron fluxes at $L = 1.5 \pm 0.02$, with the stripe thickness corresponding to a time interval of ± 15 min. Panels (b1, b2) display the total magnitude of FACs flowing in an upward direction in the Northern Hemisphere for the respective months. Panels (c1, c2) depict the Δj values over time, with color coding to indicate the total upward FACs in the Northern Hemisphere (as shown in panels b1, b2). Panels (d1, d2) present the AE index, while panels (e1–e2) represent the Sym-H index for the respective time periods.

approximately 23 MA, was recorded on 17 March 2015. This intensification corresponded with disturbances in the electron flux band-like structures shown in Figure 2a1. Additional FAC intensifications were noted on 1, 3, and 22 March 2015, peaking at around 10 MA. Figure 2c1 represents the ratio Δj . Error bars signify the standard deviation of Δj , while color codes indicate total upward FACs. Large increases in Δj were observed to coincide with FAC intensification.

Figures 2d1 and 2e1 show the AE and Sym-H index, respectively. Similar tendencies have been observed for September 2017, as detailed in Figure 2a2–2e2. Data gaps were noted in the RBSPICE electron flux on 27 September 2017 (Panel-a2) and in the AMPERE FAC magnitude on 8 September 2017 (Panel-b2). Sudden increases in Δj were also associated with spikes in FACs. Likewise, we have conducted an analysis of the electron zebra stripes for June 2015, but it is not depicted here as it shows similar characteristics.

Figure 3 shows the relationship between observed Δj and the maximum FAC magnitudes within the preceding 12 hr at any given time of electron observation for March 2015, June 2015, and September 2017. Correlation

PANDYA ET AL. 4 of 9

19448007, 2024, 3, Downloaded from https://agupubs.onlinelibrary.wiley.com/doi/10.1029/2023GL107822 by South

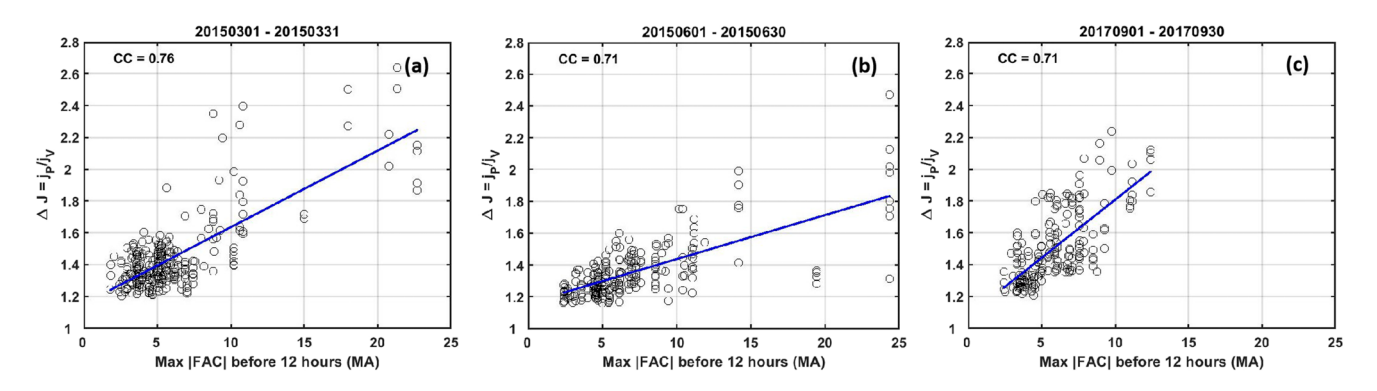


Figure 3. Relation between Δj and the maximum magnitude of upward FACs within 12 hr preceding specific observation times for electron fluxes. Data are presented for the months of (a) March 2015, (b) June 2015, and (c) September 2017.

coefficients for these months were 0.76, 0.71, and 0.71, respectively. Here, the correlation coefficients between the observed Δj and the maximum magnitude of FACs over the past 12 hr are notably strong. When the analysis was repeated with a duration shorter than 12 hr, these coefficients diminished. This reduction can be explained by the elapsed time (i.e., time spent since start) of the drifting electrons giving rise to consecutive peaks. The typical elapsed time for ~100 keV electrons is ~8–12 hr, implying that it takes several hours for electrons to travel from the outer region to L=1.5 and form zebra stripes. This observation is consistent with findings by Liu et al. (2016), who used a sinusoidal function to model the detrended electron fluxes and demonstrated that the amplitude of zebra stripes correlated maximally with the Kp index over a 12-hr interval preceding the observations.

Employing global MHD simulations of the magnetic storm on 7–8 September 2017 (Pandya et al., 2023), we obtained the azimuthal component of the ionospheric electric field (E_{ϕ}) at midnight and a magnetic latitude of 35.26° to establish the ordinate in Figure 4. This particular magnetic latitude, 35.26°, corresponds to the footpoint of the magnetic field lines in the ionosphere connected to the magnetic field line of L=1.5. We also calculated

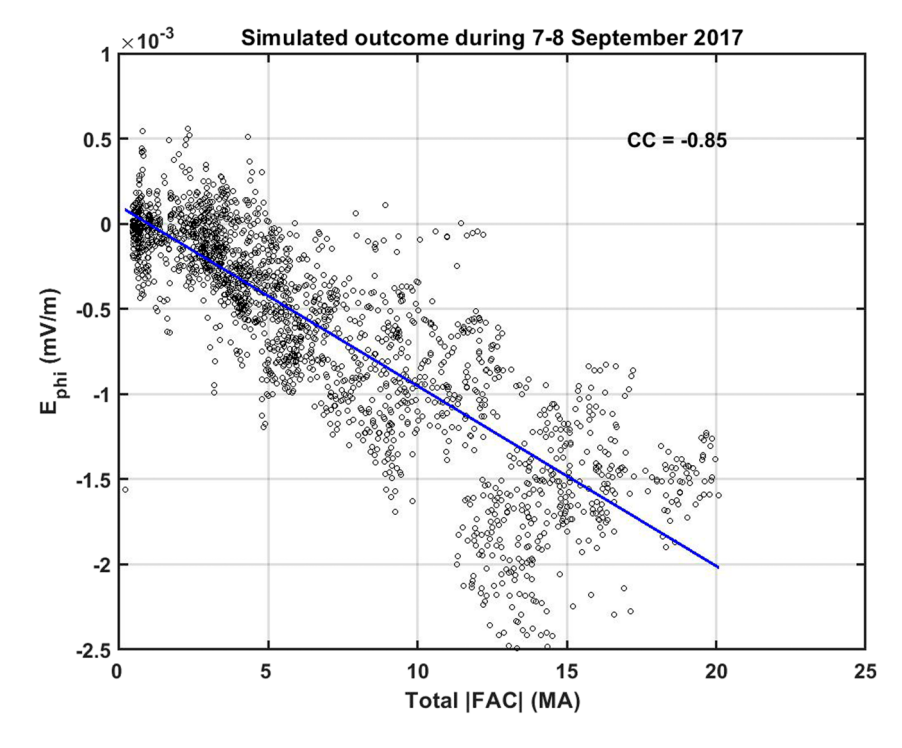


Figure 4. Relation between the azimuthal component of the electric field (E_{ϕ} , positive eastward) at midnight and the magnetic latitude of 35.26° in the ionosphere with the total amount of FACs in the ionosphere, observed on 7–8 September 2017. The data are derived from global MHD simulations.

PANDYA ET AL. 5 of 9



the total amount of the FACs integrated across all the grid points in MLT and magnetic latitudes ranging from 51° to 90° in both the hemispheres. The number of grid points are 321 in MLT and 119 in magnetic latitudes from 51° to 90°. The numbers are sufficient to capture the Region 1 and Region 2 FACs as demonstrated by Tanaka (2015) and Ebihara et al. (2014). The abscissa in Figure 4 represents the integrated magnitude of the FACs flowing into and away from the ionosphere during the interval of 1800 UT on 7 September to 1200 UT on 8 September. A negative correlation coefficient of -0.85 was found between E_{ϕ} (positive eastward) and the total amount of FACs, indicating that the westward electric field at midnight is strongly correlated with the magnitude of FACs.

4. Discussion

Based on comprehensive long-term studies using data from the Van Allen Probes spacecraft, electron zebra stripes appear to be a ubiquitous phenomenon across varying levels of geomagnetic activity. While Datlowe et al. (1985) previously highlighted the frequent appearance of multiple peaks in the South Atlantic Anomaly region, they did not report the variance in the peak-to-valley ratio under different geomagnetic conditions. Sauvaud et al. (2013) explored the relationship between drift-resonant interactions of electrons, magnetic field perturbations, and the formation of zebra stripes during active intervals. Alternatively, Ukhorskiy et al. (2014) proposed a hypothesis involving electric fields induced by electromagnetic oscillations related to Earth's rotation and dipole tilt. In the current study, we propose that enhanced FACs trigger magnetospheric convection, subsequently causing the inward drift of electrons influenced by the westward E_{ϕ} , as shown by Pandya et al. (2023), ultimately leading to the intensification of zebra stripes.

Our study reveals a strong correlation between the peak-to-valley ratio of electron fluxes and total FACs, which can be reasonably attributed to solar-wind-magnetosphere interactions. Two types of large-scale FACs are observed in the polar regions, Region 1 and Region 2 as identified by Iijima and Potemra (1978). The Region 1 FAC system consists of a poleward pair flowing into the ionosphere on the dawnside and exiting on the duskside. Increases in Region 1 FACs have been correlated with a substantial southward component of the Interplanetary Magnetic Field (IMF) (Anderson et al., 2008; Edwards et al., 2020; Papitashvilli et al., 2002; Weimer, 2001). These FACs connect to ionospheric currents to complete an electrical circuit, subsequently establishing an electric potential within the ionosphere. Region 1 FACs create a positive space charge on the dawnside and a negative space charge on the dusk side, leading to corresponding electric fields. Ground-based observations have shown that electric fields extend horizontally from the polar to equatorial regions (Kikuchi et al., 1996). This rapid propagation toward the equatorial region is likely facilitated by a waveguide mode occurring between the ionosphere and the Earth's surface (Kikuchi, 2005). It is postulated that these electric fields also extend from the ionosphere to the magnetosphere. Global MHD simulation results indicate upward Poynting flux at low latitudes toward the deep inner magnetosphere (Ebihara et al., 2020). Transient events often show an upward Poynting flux (Nishimura et al., 2010), whereas a downward Poynting flux is usually observed at high latitudes (Gary et al., 1995; Kelley et al., 1991). If the electric field originating in the mid- and low-latitude ionosphere propagates efficiently in an upward direction, it would contribute to the formation of a dawn-to-dusk convection electric field at extremely low L-shell values, such as L = 1.5. This dawn-to-dusk electric field, specifically the westward field on the nightside, drives inward $E \times B$ drift of nightside electrons, resulting in the observed zebra stripe pattern in electron fluxes (Pandya et al., 2023). The enhancement of Region 1 FACs thus naturally leads to the intensification of zebra stripes. Concurrently, hot plasma is transported from the near-Earth plasma sheet into the inner magnetosphere, fueling the development of a storm-time ring current (Ebihara & Ejiri, 2000, 2003 and references therein). This mechanism provides a plausible explanation for the intensification of zebra stripes during intense geomagnetic storms.

Lejosne and Mozer (2020) provided a detailed statistical analysis of the perturbation electric field at L values ranging from 1.5 to 2.5, a range within which zebra stripes are hypothesized to form. The electric field exhibits a westward orientation in the midnight-dawn sector and an eastward orientation on the dayside. This distribution aligns with the previously described mechanism. Additionally, the electric field is not necessarily symmetric relative to the noon-midnight meridian, owing to the asymmetric distribution of FACs and the discontinuous nature of the ionospheric Hall current. As illustrated in Figure 9 of Pandya et al. (2023), the eastward electric field intensifies in the midnight-dawn sector rather than the dusk-midnight sector, for the reasons mentioned. Therefore, the observed skewness of the perturbed electric field, as shown in Figure 9 of Lejosne and Mozer (2020), can be reasonably attributed to significant contributions from the ionosphere, supporting the outlined scenario.

PANDYA ET AL. 6 of 9

The origin of Region 1 FACs, known to result from the interaction between solar wind and Earth's magnetic field, has been a subject of longstanding debate (e.g., Bythrow et al., 1981; Iijima, 2000; Lee & Roederer, 1982). Recent work based on global MHD simulations suggests that Region 1 FACs are directly generated near the flank magnetopause, where plasma originating from solar wind pulls newly reconnected magnetic field lines (Ebihara & Tanaka, 2022). This region acts as FAC dynamo, as the plasma performs negative work against the magnetic tension force, thereby exciting Alfvén waves accompanied by FACs. Regardless of the specific generation mechanism for Region 1 FACs, it can be concluded that zebra stripes are a natural outcome of the solar wind-inner magnetospheric coupling, and magnetosphere-ionosphere (MI) with circuit completion in the ionosphere.

5. Summary

We investigated the patterns of electron zebra stripes in the deep inner magnetosphere at L=1.5, as observed by the twin Van Allen Probes during the entire months of March 2015, June 2015, and September 2017. These observations were compared with FACs recorded by AMPERE. A global MHD simulation was employed to understand the relationship between FACs and the electric field at mid-latitudes (L-value). Our key findings are summarized as follows:

- Under quiet geomagnetic conditions, the zebra stripes remained weak; however, under disturbed conditions, they underwent significant change in its magnitude. The peak-to-valley ratio of the electron flux (Δj) increased substantially.
- Δj demonstrated a strong correlation with net FACs, showing a correlation coefficient of 0.70.
- Global MHD simulation results indicated that the westward electric field around midnight in the deep inner magnetosphere is correlated well with net FACs.
- These features are reasonably explained in terms of the solar wind-magnetosphere coupling as follows. When the net FACs increase due to the southward IMF, the ionospheric currents increase to satisfy the current continuity. This results in the intensification of the convection electric field, which subsequently propagates upward into the inner magnetosphere transporting electrons inward to form zebra stripes. Consequently, the zebra stripes observed during disturbed intervals can be understood as a natural outcome of solar wind-inner magnetosphere coupling.

The phenomenon of electron zebra stripes is of immense importance in the field of space physics, particularly concerning the interactions between solar wind and planetary magnetospheres, including those of Earth, Jupiter, and Saturn. Our findings highlight the crucial role of MI coupling in shaping the characteristics of inner magnetospheric electron zebra stripes. This highlights the need to incorporate this aspect in future research focused on magnetospheres in other planetary systems with intense dipolar magnetic fields. In subsequent studies, we aim to investigate how the intensity of electron zebra stripes varies for particles that mirror off the equator, providing valuable insights into the fundamental mechanisms governing the kinetic energies of trapped electrons.

Data Availability Statement

The data on which this article is based are available in FTECS (2017) and Johns Hopkins University Applied Physics Laboratory (2017).

References

Anderson, B. J., Korth, H., Waters, C. L., Green, D. L., & Stauning, P. (2008). Statistical Birkeland current distributions from magnetic field observations by the Iridium constellation. *Annales Geophysicae*, 26(3), 671–687. https://doi.org/10.5194/angeo-26-671-2008

Anderson, B. J., Takahashi, K., Kamei, T., Waters, C. L., & Toth, B. A. (2002). Birkeland current system key parameters derived from Iridium observations: Method and initial validation results. *Journal of Geophysical Research*, 107(A6), 1–14. https://doi.org/10.1029/2001JA000080
Anderson, B. J., Takahashi, K., & Toth, B. A. (2000). Model subtraction. *Geophysical Research Letters*, 27(24), 4045–4048. https://doi.org/10.1029/2000g1000094

Breneman, A. W., Wygant, J. R., Tian, S., Cattell, C. A., Thaller, S. A., Goetz, K., et al. (2022). The Van Allen Probes electric field and waves instrument: Science results, measurements, and access to data. *Space Science Reviews*, 218(8), 69. https://doi.org/10.1007/s11214-022-00934-y Bythrow, P. F., Heelis, R. A., Hanson, W. B., Power, R. A., & Hoffman, R. A. (1981). Observational evidence for a boundary layer source of dayside region 1 field-aligned currents. *Journal of Geophysical Research*, 86(A7), 5577–5589. https://doi.org/10.1029/JA086iA07p05577

Cladis, J. B. (1966). Resonance acceleration of particles in the inner radiation belt. In *Radiation trapped in the Earth's magnetic field* (pp. 112–115). Springer. https://doi.org/10.1007/978-94-010-3553-8 9

Cowley, S. W. H. (2000). Magnetosphere-ionosphere interactions: A tutorial review.

Acknowledgments

We thank the AMPERE team and the AMPERE Science Data Center (https:// ampere.jhuapl.edu) for providing data products derived from the Iridium Communications constellation, enabled by support from the National Science Foundation. This study was supported by JSPS KAKENHI Grants 20H01960, 20H01957, and 23H05429, and Mission Research at the Research Institute for Sustainable Humanosphere (RISH), Kyoto University. This work was partially supported by NASA Goddard Space Flight Center through cooperative agreement 80NSSC21M0180, Partnership for Heliophysics and Space Environment Research (PHaSER).

PANDYA ET AL. 7 of 9

- Datlowe, D. W., Imhof, W. L., Gaines, E. E., & Voss, H. D. (1985). Multiple peaks in the spectrum of inner belt electrons. *Journal of Geophysical Research*, 90(A9), 8333–8342. https://doi.org/10.1029/ja090ia09p08333
- Ebihara, Y., & Ejiri, M. (2000). Simulation study on fundamental properties of the storm-time ring current. *Journal of Geophysical Research*, 105(A7), 15843–15859. https://doi.org/10.1029/1999JA900493
- Ebihara, Y., Ejiri, M., & Nilsson, H. (2003). Single particle simulation on the storm-time ring current formation and DST variation. Advances in Space Research, 31(4), 1051–1058. https://doi.org/10.1016/S0273-1177(02)00784-6
- Ebihara, Y., Lee, L. C., & Tanaka, T. (2020). Energy flow in the Region 2 field-aligned current region under quasi-steady convection. *Journal of Geophysical Research: Space Physics*, 125, e2019JA026998. https://doi.org/10.1029/2019JA026998
- Ebihara, Y., & Tanaka, T. (2022). Where is region 1 field-aligned current generated? *Journal of Geophysical Research: Space Physics*, 127(3), e2021JA029991. https://doi.org/10.1029/2021ja029991
- Ebihara, Y., Tanaka, T., & Kikuchi, T. (2014). Counter equatorial electrojet and overshielding after substorm onset: Global MHD simulation study. *Journal of Geophysical Research: Space Physics*, 119(9), 7281–7296. https://doi.org/10.1002/2014ja020065
- Edwards, T. R., Weimer, D. R., Olsen, N., Lühr, H., Tobiska, W. K., & Anderson, B. J. (2020). A third generation field-aligned current model. Journal of Geophysical Research: Space Physics, 125(1), e2019JA027249. https://doi.org/10.1029/2019JA027249
- FTECS. (2017). RBSPICE level 3PAP ESRHELT dataset [Dataset]. FTECS. Retrieved from https://rbspicea.ftecs.com/Level_3PAP/ESRHELT/Gary, J. B., Heelis, R. A., & Thayer, J. P. (1995). Summary of field-aligned Poynting flux observations from DE 2. Geophysical Research Letters, 22(14), 1861–1864. https://doi.org/10.1029/95g100570
- Hao, Y.-X., Sun, Y.-X., Roussos, E., Liu, Y., Kollmann, P., Yuan, C.-J., et al. (2020). The formation of Saturn's and Jupiter's electron radiation belts by magnetospheric electric fields. *The Astrophysical Journal*, 905(1), L10. https://doi.org/10.3847/2041-8213/abca3f
- Iijima, T. (2000). Field-aligned currents in geospace: Substance and significance. Magnetospheric Current Systems, Geophysical Monograph Series, 118, 107–129.
- lijima, T., & Potemra, T. A. (1978). Large-scale characteristics of field-aligned currents associated with substorms. *Journal of Geophysical*
- Research, 83(A2), 599–615. https://doi.org/10.1029/ja083ia02p00599
 Imhof, W. L., Gaines, E. E., & Reagan, J. B. (1981a). High-resolution spectral features observed in the inner radiation belt trapped electron popu-
- lation. Journal of Geophysical Research, 86(A4), 2341–2347. https://doi.org/10.1029/ja086ia04p02341
 Imhof, W. L., Gaines, E. E., & Reagan, J. B. (1981b). Observations of multiple, narrow energy peaks in electrons precipitating from the inner radi-
- Imhor, W. L., Gaines, E. E., & Reagan, J. B. (1981b). Observations of multiple, narrow energy peaks in electrons precipitating from the inner radiation belt and their implications for wave-particle interactions. *Journal of Geophysical Research*, 86(A3), 1591–1595. https://doi.org/10.1029/ja086ia03p01591
- Johns Hopkins University Applied Physics Laboratory. (2017). AMPERE data products [Dataset]. Johns Hopkins University Applied Physics Laboratory. Retrieved from https://ampere.jhuapl.edu/download/?page=derivedProductsTab
- Kelley, M. C., Knudsen, D. J., & Vickrey, J. F. (1991). Poynting flux measurements on a satellite: A diagnostic tool for space research. *Journal of Geophysical Research*, 96(A1), 201–207. https://doi.org/10.1029/90JA01837
- Kikuchi, T. (2005). Transmission line model for driving plasma convection in the inner magnetosphere. The Inner Magnetosphere: Physics and Modeling, 155, 173–179. https://doi.org/10.1029/155em20
- Kikuchi, T., Lühr, H., Kitamura, T., Saka, O., & Schlegel, K. (1996). Direct penetration of the polar electric field to the equator during DP 2 event as detected by the auroral and equatorial magnetometer chains and the EISCAT radar. *Journal of Geophysical Research*, 101(A8), 17161–17173. https://doi.org/10.1029/96ia01299
- Lee, L. C., & Roederer, J. G. (1982). Solar wind energy transfer through the magnetopause of an open magnetosphere. *Journal of Geophysical Research*, 87(A3), 1439–1444. https://doi.org/10.1029/JA087iA03p01439
- Lejosne, S., & Mozer, F. S. (2016a). Typical values of the electric drift E × B/B2 in the inner radiation belt and slot region as determined from Van Allen Probe measurements. *Journal of Geophysical Research: Space Physics*, 121(12), 12014–12024. https://doi.org/10.1002/2016JA023613
- Lejosne, S., & Mozer, F. S. (2016b). Van Allen Probe measurements of the electric drift E × B/B2 at Arecibo's L = 1.4 field line coordinate. Geophysical Research Letters, 43(13), 6768–6774. https://doi.org/10.1002/2016GL069875
- Lejosne, S., & Mozer, F. S. (2020). Experimental determination of the conditions associated with zebra stripe pattern generation in the Earths inner radiation belt and slot region. *Journal of Geophysical Research: Space Physics*, 125(7). https://doi.org/10.1029/2020ja027889
- Lejosne, S., & Roederer, J. G. (2016). The "zebra stripes": An effect of F region zonal plasma drifts on the longitudinal distribution of radiation belt particles. *Journal of Geophysical Research: Space Physics*, 121(1), 507–518. https://doi.org/10.1002/2015ja021925
- Liu, Y., Zong, Q., Zhou, X., Foster, J. C., & Rankin, R. (2016). Structure and evolution of electron zebra stripes in the inner radiation belt. *Journal of Geophysical Research: Space Physics*, 121(5), 4145–4157. https://doi.org/10.1002/2015ja022077
- Manweiler, J. W., Breneman, A., Niehof, J., Larsen, B., Romeo, G., Stephens, G., et al. (2022). Science of the Van Allen Probes science operations centers. *Space Science Reviews*, 218(8), 66. https://doi.org/10.1007/s11214-022-00919-x
- Mauk, B. H., Fox, N. J., Kanekal, S. G., Kessel, R. L., Sibeck, D. G., & Ukhorskiy, A. (2012). Science objectives and rationale for the radiation belt storm probes mission. Space Science Reviews. 179(1–4), 3–27. https://doi.org/10.1007/s11214-012-9908-y
- Mitchell, D. G., Lanzerotti, L. J., Kim, C. K., Stokes, M., Ho, G., Cooper, S., et al. (2013). Radiation belt storm probes ion composition experiment (RBSPICE). Space Science Reviews, 179(1–4), 263–308. https://doi.org/10.1007/s11214-013-9965-x
- Moriguchi, T., Nakamizo, A., Tanaka, T., Obara, T., & Shimazu, H. (2008). Current systems in the Jovian magnetosphere. *Journal of Geophysical Research*, 113(5), 1–10. https://doi.org/10.1029/2007JA012751
- Nishimura, Y., Kikuchi, T., Shinbori, A., Wygant, J., Tsuji, Y., Hori, T., et al. (2010). Direct measurements of the Poynting flux associated with convection electric fields in the magnetosphere. *Journal of Geophysical Research*, 115(A12), A12212. https://doi.org/10.1029/2010JA015491
- Pandya, M., Ebihara, Y., Tanaka, T., & Manweiler, J. W. (2023). Formation of electron zebra stripes observed on 8 September 2017. *Journal of Geophysical Research: Space Physics*, 128(4), e2022JA030950. https://doi.org/10.1029/2022JA030950
- Papitashvili, V. O., Christiansen, F., & Neubert, T. (2002). A new model of field-aligned currents derived from high-precision satellite magnetic field data. *Geophysical Research Letters*, 29(14), 28-1–28-4. https://doi.org/10.1029/2001GL014207
- Sauvaud, J.-A., Walt, M., Delcourt, D., Benoist, C., Penou, E., Chen, Y., & Russell, C. T. (2013). Inner radiation belt particle acceleration and energy structuring by drift resonance with ULF waves during geomagnetic storms. *Journal of Geophysical Research: Space Physics*, 118(4), 1723–1736. https://doi.org/10.1002/jgra.50125
- Sun, Y. X., Hao, Y. X., Roussos, E., Zong, Q. G., Liu, Y., Zhou, X. Z., et al. (2022). Zebra stripe patterns in energetic ion spectra at Saturn. Geophysical Research Letters, 49(4), e2021GL097691. https://doi.org/10.1029/2021GL097691
- Sun, Y. X., Roussos, E., Hao, Y. X., Zong, Q. G., Liu, Y., Lejosne, S., et al. (2021). Saturn's inner magnetospheric convection in the view of zebra stripe patterns in energetic electron spectra. *Journal of Geophysical Research: Space Physics*, 126(10), 1–13. https://doi.org/10.1029/2021JA029600

PANDYA ET AL. 8 of 9



Geophysical Research Letters

10.1029/2023GL107822

- Tanaka, T. (2015). Substorm auroral dynamics reproduced by advanced global magnetosphere–ionosphere (M–I) coupling simulation. In *Auroral dynamics and space weather* (pp. 177–190). https://doi.org/10.1002/9781118978719.ch13
- Terada, N., Shinagawa, H., Tanaka, T., Murawski, K., & Terada, K. (2009). A three-dimensional, multispecies, comprehensive MHD model of the solar wind interaction with the planet Venus. *Journal of Geophysical Research*, 114(9), 1–11. https://doi.org/10.1029/2008JA013937
- Ukhorskiy, A. Y., Sitnov, M. I., Mitchell, D. G., Takahashi, K., Lanzerotti, L. J., & Mauk, B. H. (2014). Rotationally driven "zebra stripes" in Earth's inner radiation belt. *Nature*, 507(7492), 338–340. https://doi.org/10.1038/nature13046
- Weimer, D. R. (2001). Maps of ionospheric field-aligned currents as a function of the interplanetary magnetic field derived from dynamics explorer 2 data. *Journal of Geophysical Research*, 106(A7), 12889–12902. https://doi.org/10.1029/2000JA000295

PANDYA ET AL. 9 of 9